CrossMark

Rare earth complexes with 3,4-dimethylbenzoic acid and 5,5′-dimethyl-2,2′-bipyridine

Synthesis, crystal structures and thermal behavior

Min-Min Zhu[1,2] · Ning Ren[3] · Jian-Jun Zhang[1,2]

Abstract

The combination of 3,4-dimethylbenzoic acid (3,4-DMHBA) and 5,5′-dimethyl-2,2′-bipyridine (5,5′-DM-2,2′-bipy) with rare earth nitrate under the room-temperature conditions results in two novel complex formulated as [Ho(3,4-DMBA)$_3$(5,5′-DM-2,2′-bipy)(H$_2$O)] (1) and [La(3,4-DMBA)$_3$(3,4-DMHBA)(5,5′-DM-2,2′-bipy)]$_2$(2), respectively. The structures were confirmed by single-crystal X-ray diffraction. Two complexes are all characterized with elemental analysis and PXRD. Interestingly enough, because of the lanthanide contraction phenomena, the complex **1** is a mononuclear molecule with the coordination number of eight, but the complex **2** is a binuclear molecule with the coordination number of nine. The thermal decomposition mechanism for two complexes was discussed by TG-DTG technology. In addition, the three-dimensional infrared accumulation spectra of the evolved gas during the thermal decomposition for title complexes were investigated via the simultaneous TG/DSC-FTIR techniques. Beyond that, the heat capacities of complexes were measured by DSC. And the smoothed value of heat capacities and thermodynamic functions (H_T-$H_{298.15}$) and (S_T-$S_{298.15}$) were calculated according to the fitted polynomial and thermodynamic equations.

Introduction

As we all know, the rare earth industry in China is huge and important domestically elsewhere around the world [1–3]. Because of the unique 4f electronic energy level

✉ Ning Ren
ningren9@163.com

✉ Jian-Jun Zhang
jjzhang6@126.com

1 Testing and Analysis Center, Hebei Normal University, Shijiazhuang 050024, People's Republic of China

2 College of Chemistry and Material Science, Hebei Normal University, Shijiazhuang 050024, People's Republic of China

3 College of Chemical Engineering and Material, Handan University, Handan 056005, People's Republic of China

structure and effective transitions of 4f–4f and 5d–4f, the lanthanide ions are known to possess many attractive properties such as magnetic materials, long lifetimes, catalysts, ligand-dependent sensitization, thermodynamics, and high conversion efficiency [4–7]. It is generally known that trivalent lanthanide ions possess high coordination numbers and more diverse coordination environment. And compared with other lanthanide complexes structures, the Ln^{3+} complexes based on aromatic carboxylic acids show more excellent mechanical flexibility, more outstanding film-forming capability and better processability, so aromatic carboxylic acids are usually used as a class of excellent organic ligands. This makes the lanthanide complexes present a variety of coordination modes, such as monodentate, chelating, bridging and bridging-cheating [8–10]. On the other hand, in recent years, we have been devoted to explore the construction of coordination polymers applying ligands with increased flexibility. Among these ligands, N-containing heterocyclic auxiliary ligands

have higher thermal stability and stronger luminescence, for example, 5,5′-dimethyl-2,2′-bipyridine.

In this paper, the 3,4-dimethylbenzoic acid (3,4-DMHBA) was chosen as the first ligand and 5,5′-dimethyl-2,2′-bipyridine (5,5′-DM-2,2′-bipy) was selected as ancillary ligand to coordinate with Ln(III) ions. And we have successfully synthesized two novel innovative lanthanide complexes [Ho(3,4-DMBA)₃(5,5′-DM-2,2′-bipy)(H₂O)] (1) and [La(3,4-DMBA)₃(3,4-DMHBA)(5,5′-DM-2,2′-bipy)]₂ (2). Because of the lanthanide contraction phenomena, the structures of two complexes are very different. In addition, two complexes can be all assembled into a 1D and 2D supramolecular structure. What is more, the thermal decomposition mechanism of title complexes was investigated via the TG/DSC-FTIR technology. And the heat capacities of complexes were measured by DSC. Finally, the thermodynamic parameters, the enthalpy and entropy of the title complexes relative to the standard reference temperature 298.15 K were calculated.

Experimental

Materials and general methods

All reagents and solvents were purchased from Beijing InnoChem Science & Technology Co., Ltd., at a high purity and used as received without further purification. Element analyses (C, H and N) were measured with the Vario-EL II element analyzer, and the metal content was obtained using an EDTA titration method. Single-crystal X-ray diffraction data were collected by Smart 100 diffractometer with graphite monochromatic Mo Kα ($\lambda = 0.71073$ Å and $\lambda = 1.54178$ Å) at 298(2) and 293(2) K. The structures were solved using SHELXS-97 program (direct methods) and refined with full-matrix least squares on F^2 using the SHELXS-97 program. And the powder X-ray diffraction was measured by a Bruker D8 ADVANCE X-ray diffraction over the scanning range of 5–50° (2θ) with Cu K radiation ($\lambda = 0.71073$ Å) at 298(2).

The thermogravimetric (TG), differential thermogravimetric (DTG), differential scanning calorimetric (DSC) and Fourier transform infrared (FTIR) analyses of title complexes were carried out under a simulated air atmosphere at a heating rate of 10 K min^{-1} by a TG/DSC-FTIR system, which was the combination of a NETZSCH STA 449F3 instrument and a Bruker TENSOR 27 Fourier transform infrared spectrometer.

Synthesis

A mixture solution composed of 3,4-DMHBA (0.06 mmol), 5,5′-DM-2,2′-bipy (0.02 mmol) and 95%

ethanol (6 mL) was adjusted by the prepared NaOH solution (1 mol L^{-1}) over the pH range of 5–7. Then, the mixture solution was added dropwise into 3-mL aqueous solution of Ln(NO₃)₃·6H₂O (0.02 mmol) under stirring and deposit them for 12 h. The powder of complexes was obtained by filtration and drying, and the single-crystals were acquired via the method of solution evaporation at room temperature. Element analysis for C₃₉H₄₁N₂O₇Ho (%), Calcd: C, 57.50; H, 5.07; N, 3.44; Ho, 20.24. Found: C, 57.57; H, 5.05; N, 3.48; Ho, 20.27. For C₉₆H₉₈N₄O₁₆La₂(%),Calcd: C, 62.61; H, 5.36; N, 3.04; La, 15.09. Found: C, 62.63; H, 5.38; N, 3.00; La, 15.09.

Results and discussion

Description of the structures

The single-crystal X-ray structures of two types of complexes were determined. The most important crystallographic data and selected bond lengths for title complexes are listed in Tables 1 and 2, respectively. Obviously, because of the lanthanide contraction phenomena, different central ions result in different crystal parameters and structures. In order to make a comparison, the structures of single-crystal complexes 1 and 2 will be described in detail, respectively.

[Ho(3,4-DMBA)₃(5,5′-DM-2,2′-bipy)(H₂O)]

Based on the analysis of single-crystal XRD, the single crystal of [Ho(3,4-DMBA)₃(5,5′-DM-2,2′-bipy)(H₂O)] is mononuclear molecule and crystallizes in the triclinic with $P\bar{1}$ space group. Each asymmetric unit consists of one Ho(III) ion, three 3,4-DMBA⁻ ligands, one 5,5′-DM-2,2′-bipy ligand and one coordinated water (Fig. 1a). The central Ho(III) ion is eight-coordinated with six oxygen atoms (O1, O2, O3, O4, O5 and O7) and two nitrogen atoms (N1 and N2), which is consistent with the element analysis. Four oxygen atoms (O1, O2, O3 and O4) are from two bidentate chelating 3,4-DMBA⁻ ligands with the average Ho–O bond distance of 2.379 Å. The remaining two oxygen atoms (O5 and O7) are from one monodentate 3,4-DMBA⁻ ligand and a coordinated water molecule with the distance of Ho–O bond over the range of 2.235–2.339 Å. The two nitrogen atoms are from one bidentate chelating 5,5′-DM-2,2′-bipy ligand with Ho–N distances in the range of 2.496–2.526 Å. All these above display a distorted triangular dodecahedral geometry (Fig. 1b) [11–13].

It is worth mentioning that two adjacent Ho(III) ions can be linked via two strongly identical O–H···O hydrogen bonding interactions to generate a binuclear building unit [14, 15], and the binuclear building unit will be as the minimum unit of one-dimensional chain (Fig. 2a, b). Then,

Table 1 Crystallographic data and structure refinement for title complexes at pressure 101.3 kPa

Complex	1	2
Molecular formula	$C_{39}H_{41}HoN_2O_7$	$C_{96}H_{98}La_2N_4O_{16}$
M (g mol^{-1})	814.67	1841.60
T/K	293(2)	298(2)
Wavelength/Å	1.54178	0.71073
Crystal system	Triclinic	Monoclinic
Space group	$P\bar{1}$	$P2(1)/n$
a/Å	8.9266(6)	14.1072(12)
b/Å	12.8879(8)	15.7992(13)
c/Å	16.4513(11)	19.8315(18)
α/(°)	75.8590(10)	90
β/(°)	80.917(2)	91.6680(10)
γ/(°)	84.382(2)	90
Volume/Å^3	1808.8(2)	4418.2(7)
Z, calculated density/Mg m^{-3}	2, 1.496	2, 1.384
Absorption coefficient/mm^{-1}	4.501	1.021
$F(000)$	824	1888
Crystal size/mm^3	0.16 × 0.14 × 0.08	0.30 × 0.19 × 0.17
θ range for data collection/°	3.54–66.05	2.17–25.02
Limiting indices	$-9 \leq h \leq 10$	$-16 \leq h \leq 15$
	$-11 \leq k \leq 15$	$-18 \leq k \leq 18$
	$-18 \leq l \leq 19$	$-23 \leq l \leq 17$
Reflections collected/unique	11,342/6310	21,875/7787
	[$R_{(int)}$ = 0.0503]	[$R_{(int)}$ = 0.0789]
Completeness to θ = 66.05° or θ = 25.02°	99.8%	99.7%
Max. and min. transmission	0.7147 and 0.5329	0.8455 and 0.7492
Data/restraints/parameters	6310/0/525	7787/0/532
Goodness-of-fit on F^2	1.088	1.075
R_1	0.0501	0.0480
wR_2	0.1142	0.0841
R_1 (all data)	0.0702	0.1007
wR_2 (all data)	0.1254	0.1129
Largest diff. peak and hole/(e Å^{-3})	0.555 and $-$0.763	1.926 and $-$0.684

Table 2 Selected bond lengths of complexes **1** and **2**

Complex **1**	Bond length/Å	Complex **2**	Bond length/Å
Ho(1)–O(5)	2.235(4)	La(1)–O(1)#1	2.445(3)
Ho(1)–O(7)	2.339(4)	La(1)–O(5)	2.486(3)
Ho(1)–O(4)	2.359(4)	La(1)–O(3)	2.504(3)
Ho(1)–O(3)	2.366(4)	La(1)–O(4)#1	2.505(3)
Ho(1)–O(1)	2.368(4)	La(1)–O(7)	2.531(4)
Ho(1)–O(2)	2.423(4)	La(1)–O(2)	2.538(3)
Ho(1)–N(1)	2.496(4)	La(1)–N(2)	2.724(4)
Ho(1)–N(2)	2.526(4)	La(1)–N(1)	2.768(4)
		La(1)–O(1)	2.836(3)
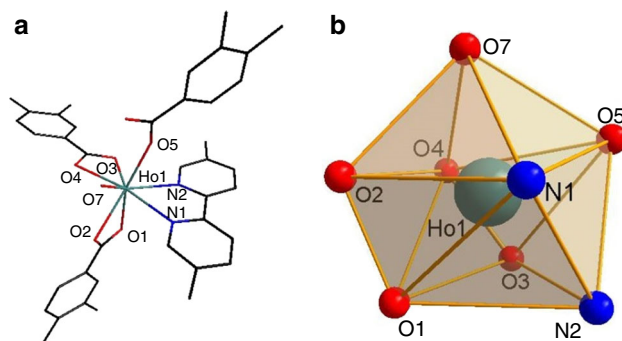
Fig. 1 a Crystal structure of complex **1** and **b** coordination geometry of Ho (III) ion

the binuclear units are further connected by the other two identical C–H···O hydrogen bonding interactions to assemble the molecules into a one-dimensional chain

supramolecular structure along c-axis direction (Fig. 3). Finally, the 2D network structure is furthermore stabilized by π···π stacking interactions (Fig. 4).
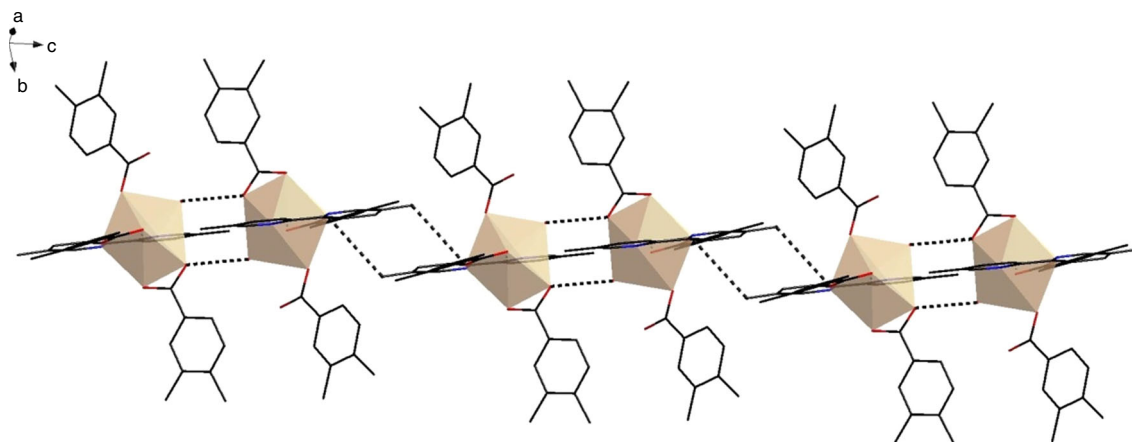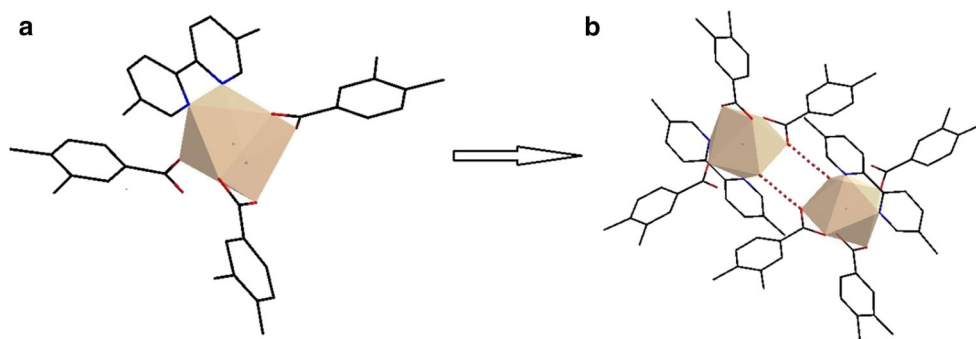
Fig. 3 1D chain structure of complex **1** along the *c*-axis

[La(3,4-DMBA)₃(3,4-DMHBA)(5,5′-DM-2,2′-bipy)]₂

Single-crystal X-ray structure analysis shows that complex
2 is a novel binuclear molecule with the monoclinic *P*2(1)/
n space group, which is different from that of the complex
1. It is interesting that the binuclear molecule is made up of
two La(III) ions, six deprotonated 3,4-DMBA⁻ ligands,
two unprotonated 3,4-DMHBA ligands and two 5,5′-DM-

2,2′-bipy ligands, which is rarely reported before (Fig. 5a).
The carboxylic groups in complex **2** adopt three different
coordination modes: monodentate, bridging bidentate and
bridging tridentate (Fig. 6) [16, 17]. The coordination
environment of the central La(III) ion is nine-coordinated
with seven oxygen atoms (O1, O1A, O2, O3, O4, O5 and
O7) and two nitrogen atoms (N1 and N2), which exhibits a
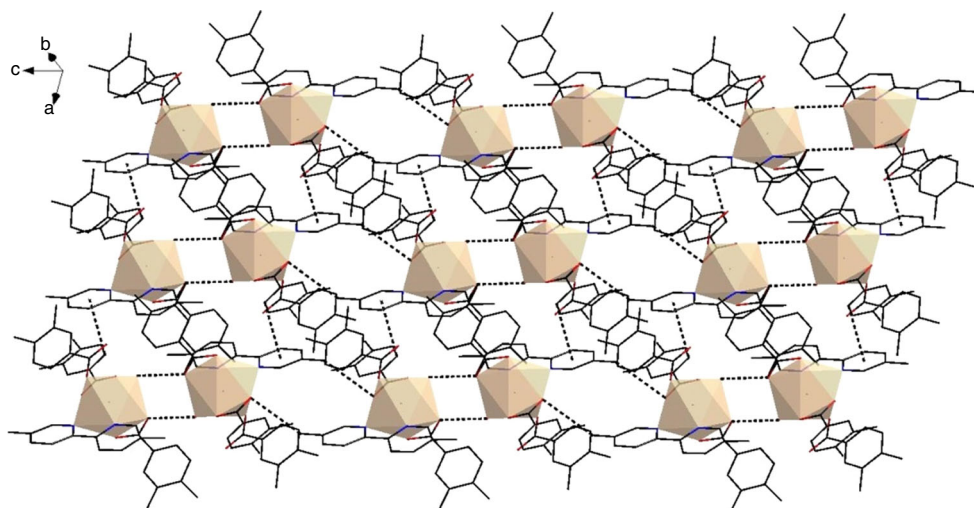distorted monocapped square antiprismatic coordination

Fig. 5 a Crystal structure of complex **2** and **b** coordination geometry of La (III) ion
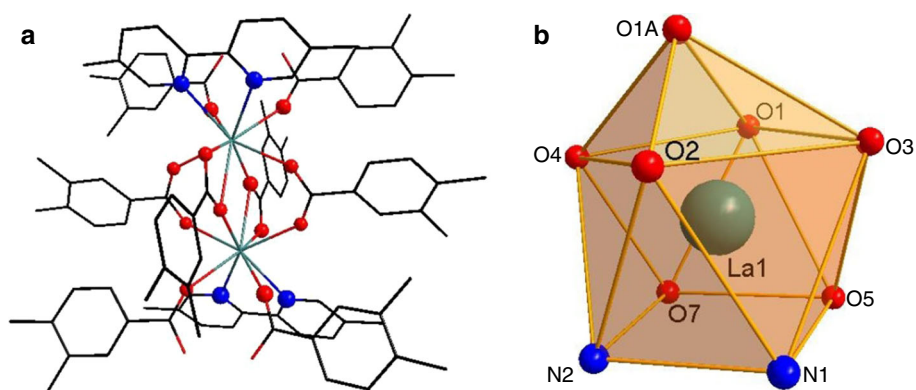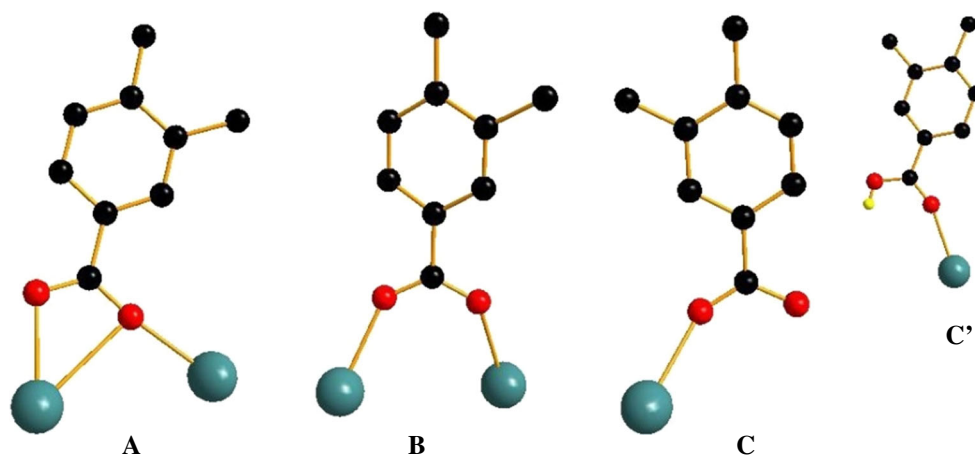

Fig. 6 Coordination modes of 3,4-DMBA⁻ ligand for complex **2**

geometry (Fig. 5b). The average length of La–O is 2.549 Å, and the average distance of La–N bonds is 2.649 Å. In short, we can see that the average bond distance of La–O is shorter than that of La–N. Thus, it has been considered to the result of 5,5′-DM-2,2′-bipy ligand is always lost earlier than 3,4-DMBA⁻ in thermal decomposition process [18, 19].

As shown in Fig. 7, the packing diagram of complex **2** was linked as supramolecular 1D chain via two strongly same offset face-to-face π···π stacking interactions from

two six-membered rings of 5,5′-DM-2,2′-bipy ligands along *a*-axis direction.

Then, the chains were assembled via C–H···O hydrogen bonds interactions to form a 2D network supramolecular structure along ab plane (Fig. 8).

X-ray powder diffraction

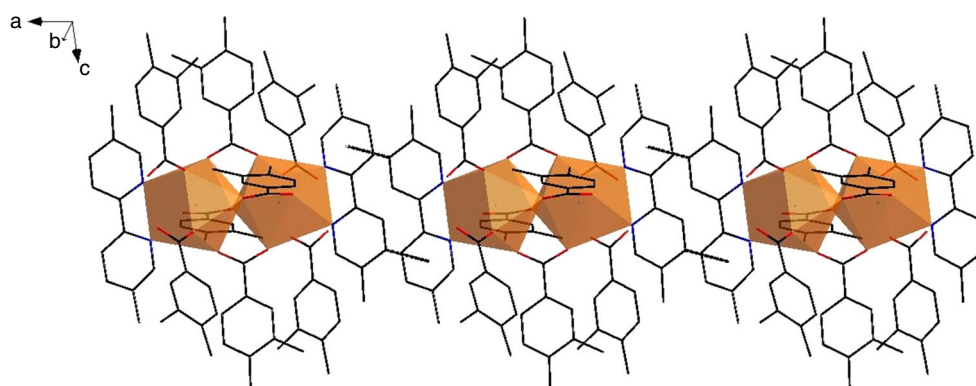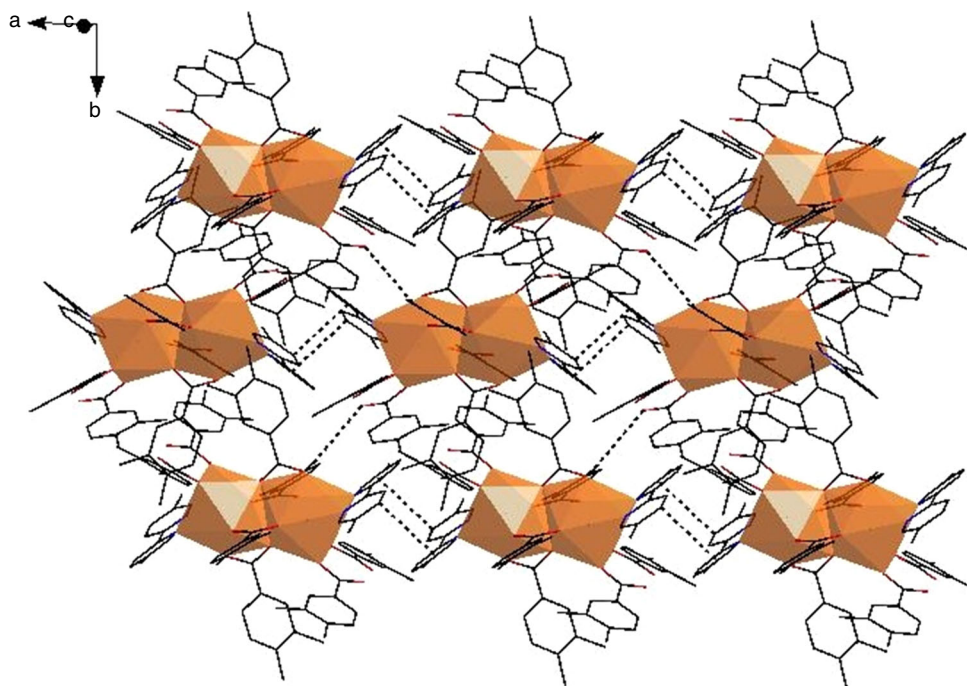Figure 9a, b shows the powder X-ray diffraction (PXRD) patterns of the complexes and ligands, which compared

Fig. 7 1D chain structure of complex **2** along the *a*-axis by π···π stacking interactions

with the corresponding simulated single-crystal diffraction data, respectively. It can be clearly seen that the diffraction peaks of the complexes **1** and **2** are different from that of the ligands in the aspect of numbers, location and intensity, indicating that the two complexes are not the mechanical adduct of the ligands peaks, that is to say, new phases have been produced. Beyond that, the curves of complexes **1** and **2** are essentially in agreement with the simulated ones, respectively, suggesting the pure samples of complexes **1** and **2**.

Thermal analysis

TG/DTG-DSC thermoanalytical methods are regarded as one of the most important characterization methods that explore the chemical changes and physical changes of single crystal in the aspect of chemical phenomenon like dehydration, oxidation reduction decomposition and physical phenomenon such as vaporization, absorption and adsorption sublimation [20]. Thermal analysis of title complexes was investigated at a heat rate of 10 K min^{-1} in the temperature range of 300–1200 K under a simulated air atmosphere. The title complexes are stable at room temperature, and begin to decompose gradually with the increase in temperature. Thermal curves TG/DTG-DSC for title complexes are shown in Fig. 10a, b, and the data of thermal analysis are listed in Table 3.

The TG curve of the complex **1** has three-step mass loss processes (Fig. 10a). The first step occurs over the temperature range of 379.15–395.15 K with a mass loss of

2.21% against theoretical mass loss 2.19%, which belongs to the dehydration with a small endothermic peak in DSC curve (Tp = 391.55 K; ΔH = 33.67 J g^{-1}) [21]. The second step takes place between 395.15 and 609.15 K with a mass loss of 22.58% against theoretical mass loss 22.61%, accounting for the loss of one 5,5′-DM-2,2′-bipy, meanwhile, the DSC measurements show an exothermic peak (Tp = 466.45 K; ΔH = − 147.7 J g^{-1}). The last mass loss process is the decomposition of 3,4-DMBA$^-$ ligands (Calcd: 51.65%; Found: 51.99%) in the temperature from 609.15 to 984.15 K with a evident big exothermic peak in DSC curve (Tp = 838.35 K; ΔH = − 4887 J g^{-1}). Finally, the complex 1 is completely decomposed into the metal oxides (Ho$_2$O$_3$) with mass percentage of 23.58% against theoretical mass of 23.19%.

For complex **2**, there are two stages in the thermal decomposition processes (Fig. 8b). The first stage of weightlessness is mainly ascribed to the removing of 5,5′-DM-2,2′-bipy and part of the 3,4-DMBA$^-$(or 3,4-DMHBA) (Calcd: 34.28%) over the temperature from 338.15 to 562.15 K with an exothermic peak (Tp = 471.85 K; ΔH = 191.6 J g^{-1}) on DSC curve. The second stage of weightlessness is on account of the remaining 3,4-DMBA$^-$ ligands (Calcd: 47.61%) between the 562.15 and 1249.15 K with a obvious big exothermic peak (Tp = 818.55 K; ΔH = − 5031 J g^{-1}) according to the DSC curve. Leaving behind the residue is La$_2$O$_3$. In the end, the total mass percentage of 81.89% was consistent well with the theoretical mass of 82.31%.
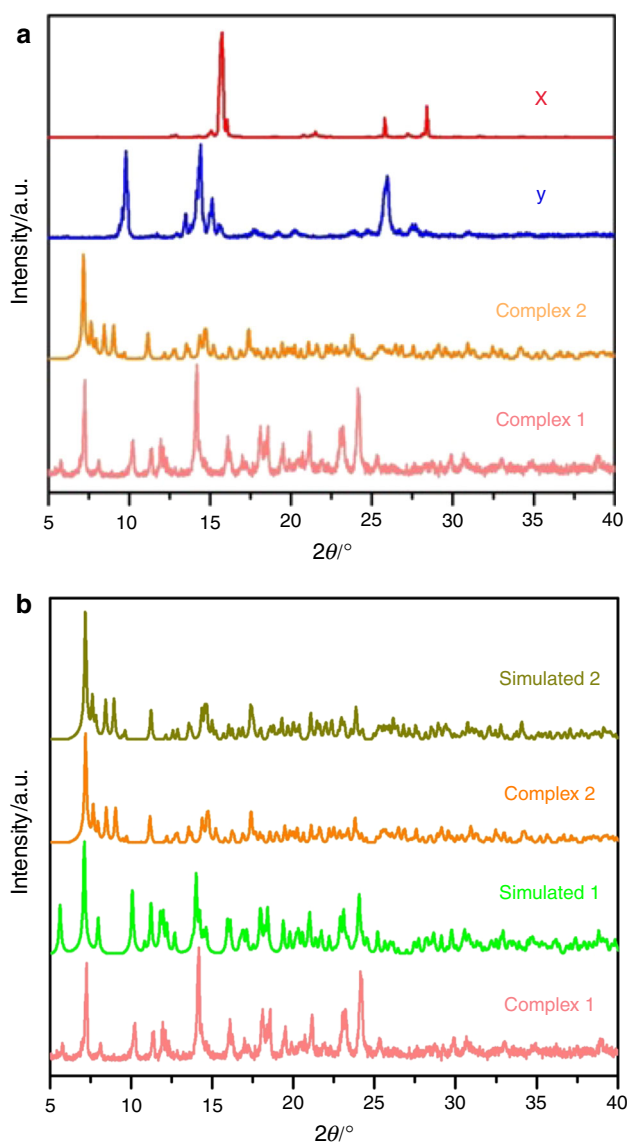
Fig. 9 a Experimental PXRD patterns of complexes **1** and **2** and ligands (x5,5′-DM-2,2′-bipy 3,4-DMHBA;) and **b** experimental and simulated PXRD patterns of complexes **1** and **2**

FTIR

Stacked plots of the FTIR spectra and signal infrared spectrograms of the evolved gas products for title complexes during the thermal decomposition under simulated air atmosphere were worked out and are shown in Fig. 11a, b. Because the decomposition processes for title complexes are different, the complexes **1** and **2** will be researched in detail.

For complex **1**, in the first step at 390.15 K, the IR spectra of evolved gaseous products show two main absorption bands $(3431–3951, 1283–1572)$ cm^{-1} only for the coordination water decomposition. In the second FTIR spectra at 478.15 K, the characteristic doublet bands over
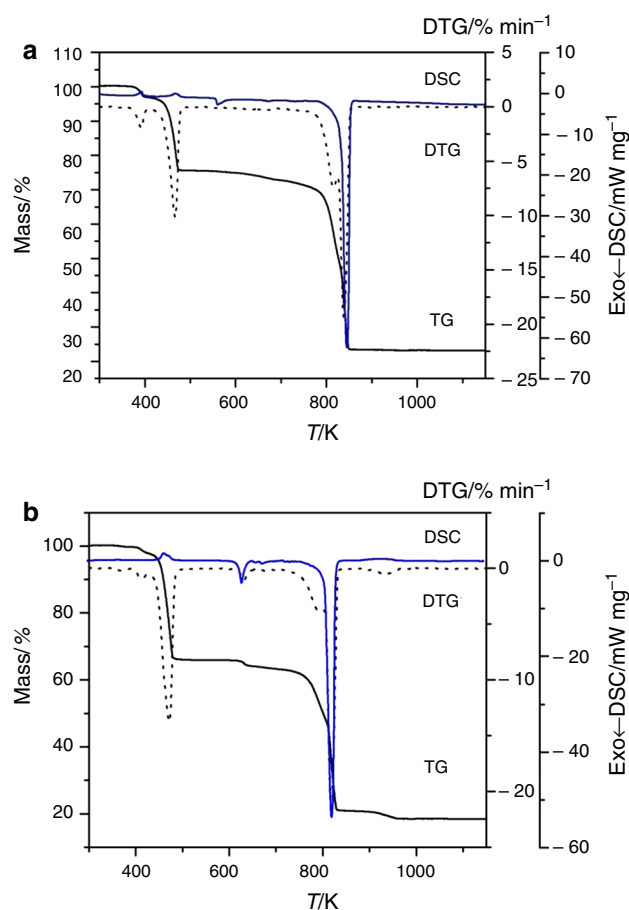

Fig. 10 TG/DTG/DSC curves of complex **1** (**a**) and complex **2** (**b**)

the range $2263–2399$ cm^{-1} and 653 cm^{-1} were observed, assigned to the stretching asymmetric and bending vibrations of carbon dioxide molecules; and some other characteristic absorption bonds are also observed such as $\nu_{C=C}$ at $(1433–1678)$ cm^{-1}, $\nu_{C–N}$ at (1373) cm^{-1}, $\nu_{C–H}$ at $(2838–3129)$ cm^{-1} and $\gamma_{C–H}$ at $(769–869)$ cm^{-1}. In addition, there is still some small molecular absorption, for example, H_2O $(3581–3899)$ cm^{-1}. In the last FTIR spectra at 846.15 K, we can see the obvious strong absorption bands of CO_2 $(2213–2404$ and $668)$ cm^{-1}, which suggests that the decomposition of the 3,4-DMBA$^-$ becomes the main contribution of the CO_2 signal. Besides, some bands of gaseous organic molecules fragments were found in the FTIR spectra, which may be due to the undecomposed ligands.

For complex **2**, there are only two characteristic absorption processes as shown in Fig. 12a, b. However, the typical characteristic absorption peaks of complex **2** are similar to that of complex **1**; therefore, complex **2** will not be studied in detail.

Table 3 Thermal analysis results of complexes **1** and **2** at pressure 101.3 kPa

Complexes	Steps	Temperature range/K	DTG Tp/K	Mass loss rate/% Found	Mass loss rate/% Calcd	Probable expelled groups	Intermediate and residue
1	I	379.15–395.15	391.55	2.19	2.21	H_2O	[Ho(3,4–DMBA)$_3$5,5′–DM–2,2′–bipy]
	II	395.15–609.15	466.45	22.58	22.61	5,5′–DM–2,2′–bipy	[Ho(3,4–DMBA)$_3$]
	III	609.15–984.15	838.35	51.65	51.99	3(3,4–DMBA$^-$)	Ho_2O_3
				76.42	76.81		
2	I	338.15–562.15	471.85	34.28	–	2(5,5′–DM–2,2′–bipy) + x(3,4–DMBA$^-$)	[La(3,4–DMBA)$_{4-x}$]$_2$
	II	562.15–1249.15	818.55	47.61	–	8–x(3,4–DMBA$^-$)	La_2O_3
				81.89	82.31		

Molar heat capacities, molar enthalpies and entropies

The experimental molar heat capacities of title complexes were obtained via adiabatic calorimeter in the temperature range from 253.15 to 345.15 K at a heating rate of 10 K min^{-1} under the nitrogen atmosphere in Table 4. From Fig. 13, it is not difficult to find that the curves of two complexes are all smooth, indicating no phase transformation or thermal abnormality [22, 23]. In addition, Fig. 13 shows that the average molar heat capacity of the complexes increased with the increase in temperature, which may be the result of the molecular vibrations. As a result, the title complexes are all stable in this area. What is more, at the same temperature the $C_{p,m}$ of complex **2** is higher than that of the complex **1**, that is because that the molar mass of binuclear molecules is higher than that of mononuclear molecules and not newly added other ligands, indicating that the molecular vibration is the most important contribution of the heat capacity [24].

The average molar heat capacities were fitted to the following polynomial equations with the reduced temperature (χ) by the method of least squares ($x = [T - (T_{max} + T_{min})/2]/[(T_{max} - T_{min})/2]$), where the T means the experimental temperature, T_{max} stands for the highest temperature and T_{min} stands for the lowest temperature.

Complex 1 [Ho(3,4-DMBA)$_3$(5,5′-DM-2,2′-DIPY)(H$_2$O)]

$$C_{p,m}/\text{J mol}^{-1}\text{ K}^{-1} = 792.76872 + 100.96462x$$
$$+ 94.76276x^2 + 67.75555x^3$$
$$- 231.61254x^4 - 128.08016x^5$$
$$+ 324.4738x^6 + 86.74624x^7$$
$$- 162.27101x^8$$

$R^2 = 0.99996 \quad SD = 0.29552$

Fig. 11 a Stacked plot of the FTIR spectra of the evolved gases for complex **1** and **b** FTIR spectra of the evolved gases of thermal decomposition of complex **1** at different temperatures
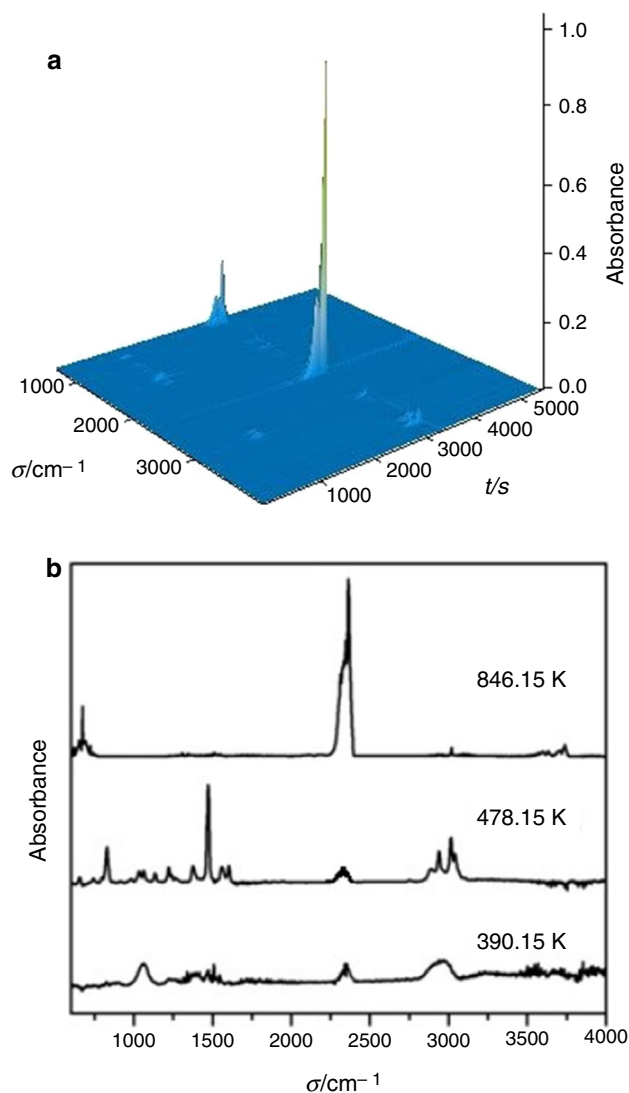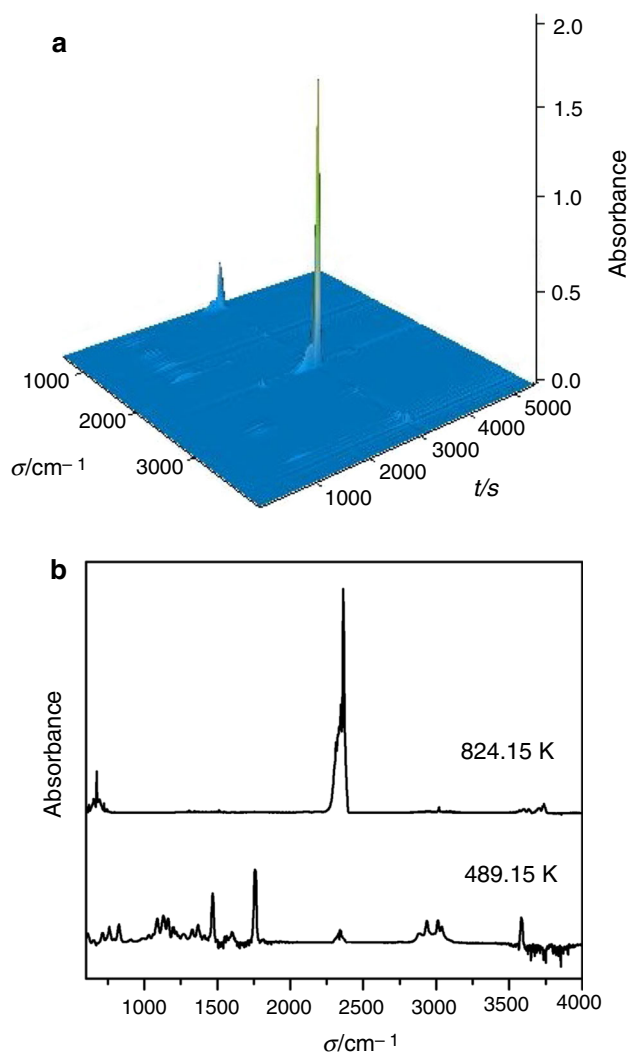
a

b

824.15 K

489.15 K

Fig. 12 a Stacked plot of the FTIR spectra of the evolved gases for complex **2** and **b** FTIR spectra of the evolved gases of thermal decomposition of complex **2** at different temperatures

Complex 2 [La(3,4-DMBA)₃(3,4-DMHBA)(5,5′-DM-2,2′-DIPY)₂]₂

$$C_{p,m}/J\ mol^{-1}\ K^{-1} = 1823.11559 + 64.93533x$$
$$-9.41469x^2 - 10.19167x^3 + 2.2076x^4$$
$$+ 45.03913x^5 - 22.48063x^6$$
$$-18.67954x^7 + 9.25713x^8$$

$$R^2 = 0.99985 \quad SD = 0.94365$$

In the above, R^2 stands for the correlation and SD stands for the standard deviation. Then, the fitting polynomial equations and the following thermodynamic equations relative to the standard reference temperature 298.15 K, are used to calculated the smoothed molar heat capacities and thermodynamic functions of complexes **1** and **2**, and

Table 4 Experimental molar heat capacities of complexes **1** and **2**

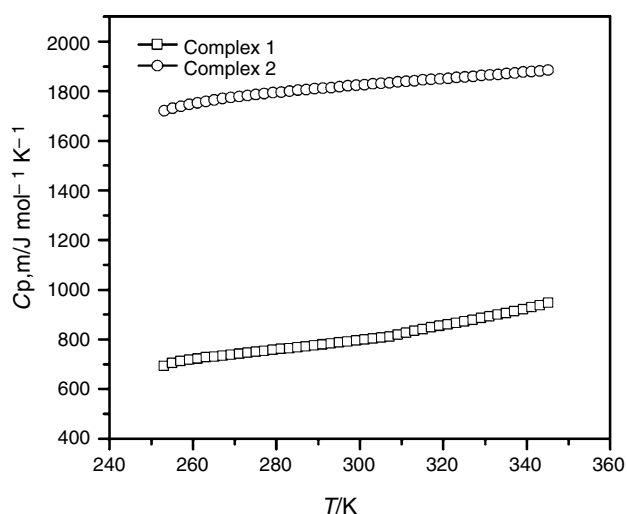| T/K	Complex **1** $C_{p,m}$/J mol⁻¹ K⁻¹	Complex **2** $C_{p,m}$/J mol⁻¹ K⁻¹
253.15	690.75	1721.27
255.15	703.31	1730.05
257.15	711.63	1738.12
259.15	717.59	1745.43
261.15	722.14	1752.11
263.15	726.09	1758.24
265.15	729.86	1763.97
267.15	733.51	1769.26
269.15	737.41	1774.11
271.15	741.22	1778.55
273.15	745.06	1782.59
275.15	748.50	1786.34
277.15	752.16	1789.87
279.15	755.91	1793.24
281.15	759.77	1796.56
283.15	763.58	1799.79
285.15	767.31	1802.88
287.15	771.08	1805.79
289.15	774.61	1808.60
291.15	778.08	1811.40
293.15	781.87	1814.29
295.15	785.72	1817.27
297.15	789.64	1820.30
299.15	793.39	1823.24
301.15	797.46	1826.11
303.15	801.76	1828.89
305.15	805.93	1831.56
307.15	810.94	1834.09
309.15	817.41	1836.57
311.15	825.37	1839.05
313.15	832.97	1841.61
315.15	839.91	1844.20
317.15	846.64	1846.79
319.15	852.88	1849.33
321.15	859.12	1851.81
323.15	865.50	1854.29
325.15	871.57	1856.82
327.15	877.60	1859.43
329.15	884.09	1862.10
331.15	890.94	1864.78
333.15	898.24	1867.47
335.15	905.38	1870.17
337.15	913.06	1872.91
339.15	921.11	1875.69
341.15	928.90	1878.47
343.15	937.13	1881.19
345.15	945.62	1883.89

Fig. 13 Experiment molar heat capacities of complexes **1** and **2** at different temperatures

the data with an interval of 2 K are listed in Tables S1 and S2.

$$H_T - H_{298.15} = \int_{298.15}^{T} C_{p,m} \mathrm{d}T$$

$$S_T - S_{298.15} = \int_{298.15}^{T} C_{p,m} T^{-1} \mathrm{d}T$$

Conclusions

The reactions of rare earth nitrate with the 3,4-DMHBA and 5,5′-DM-2,2′-bipy synthesized two novel lanthanide complexes [Ho(3,4-DMBA)$_3$(5,5′-DM-2,2′-bipy)(H$_2$O)] (1); [La(3,4-DMBA)$_3$(3,4-DMHBA)(5,5′-DM-2,2′-bipy)]$_2$(2). The complex **1** is mononuclear molecule with a coordination number of eight, which act in a distorted triangular dodecahedral geometry, while the complex **2** is binuclear molecule with the coordination number of nine, displaying a distorted monocapped square antiprismatic coordination geometry. In addition, each central La(III) ion of complex **2** was coordinated by three deprotonated 3,4-DMBA$^-$, one unprotonated 3,4-DMHBA and one 5,5′-DM-2,2′-bipy, which has rarely been reported before. The thermal decomposition mechanism for two complexes was discussed by TG-DTG technology. In addition, the three-dimensional infrared accumulation spectra of the evolved gas during the thermal decomposition for title complexes were investigated via the simultaneous TG/DSC-FTIR techniques. Beyond that, the heat capacities of complexes were measured by DSC. The smoothed value of heat capacities and thermodynamic functions (H_T-$H_{298.15}$) and (S_T-$S_{298.15}$) were calculated according to the fitted polynomial and thermodynamic equations.

Supporting information

The numbers of the two complexes (CCDC 1832477 (**1**), CCDC 1832478 (**2**)) contain the supplementary crystallographic data for this paper, which can be obtained free of charge from the Cambridge Crystallographic Data Centre via www.ccdc.cam.ac.uk/data_request/cif.

References

1. Ruan L, Gao X, Zhao J, Xu C, Liang D. Preparation and characteristics of Eu(DBM)$_3$phen: synthesis, single-crystal structure and spectroscopic analysis. J Mol Struct. 2017;1149:265–72.

2. Zong GC, Huo JX, Ren N, Zhang JJ, Qi XX, Gao J, Geng LN, Wang SP, Shi SK. Preparation, characterization and properties of four new trivalent lanthanide complexes constructed using 2-bromine-5-methoxybenzoicacid and 1,10-phenanthroline. Dalton Trans. 2015;44:14877–86.

3. Huo JX, Song SW, Jin CW, Ren N, Geng LN, Zang JJ. Synthesis, characterization, thermal decomposition mechanism and properties of the [Eu(4-MOBA)$_3$(terpy)(H$_2$O)]$_2$ complex. Acta Phys Chim Sin. 2016;32(4):901–6.

4. Zhong GQ, Li D, Zhang ZP. Hydrothermal synthesis, crystal structure and magnetic property of a homodinuclear ternary coordination polymer of nickel(II). Polyhedron. 2016;111:11–5.

5. Chesnokov GA, Topchiy MA, Asachenko AF, Muravyev NV, Grishin LI, Nikiforova AS, Utochnikova VV, Rybakov VB, Khrustalev VN, Nechaev MS. Rare-earth complexes with the 5,5′-bitetrazolate ligand-synthesis, structure, luminescence properties, and combustion catalysis. Eur J Inorg Chem. 2018;2018(6):805–15.

6. Mukherjee D, Hollerhage T, Leich V, Spaniol TP, Englert U, Maron L, Okuda J. The nature of the heavy alkaline earth metal-hydrogen bond: synthesis, structure, and reactivity of a cationic strontium hydride cluster. J Am Chem Soc. 2018;140(9):3403–11.

7. Ma MJ, Li CC, Shu DK, Wang CH, Xi P. Synthesis and characterization of bright green terbium coordination complex derived from 1,4-bis(carbonylmethyl)terephthalate: structure and luminescence properties. Spectrochim Acta A Mol Biomol Spectrosc. 2018;190:68–75.

8. Hou XY, Wang X, Gao LJ, Fu F, Wang JJ, Cao J. Synthesis, structures, luminescence, and magnetic properties of two three-dimensional lanthanide organic frameworks comprising pyrazine-2,3-dicarboxylic acid. Z Anorg Allg Chem. 2014;640(10):2072–7.

9. Ryan AJ, Darago LE, Balasubramini SG, Chen GP, Ziller JW, Furche F, Long JR, Evans WJ. Synthesis, structure, and magnetism of tris(amide) {Ln[N(SiMe$_3$)$_2$]$_3$}$^{1-}$ complexes of the non-traditional +2 lanthanide ions. Chemistry. 2018. https://doi.org/10.1002/chem.201800610.

10. Xiao YH, Deng ZP, Zhu ZB, Huo LH, Gao S. Rare earth metal-organic complexes constructed from hydroxyl and carboxyl modified arenesulfonate: syntheses, structure evolutions, and

ultraviolet, visible and near-infrared luminescence. Dalton Trans. 2017;46(47):16493–504.

11. Lymperopoulou S, Lazarides T, Papachristodoulou C, Raptopoulou CP, Psycharis V, Plakatouras JC. Synthesis, structural characterization, and fluorescence of a series of 1D rare earth coordination polymers with a substituted iminodiacetate ligand. Inorg Chim Acta. 2018;472:276–82.

12. Sun J, Zhang MH, Wang AY, Cai ZW. Synthesis, crystal structure, gas absorption, and separation properties of a novel complex based on Pr and a three-connected ligand. Crystals. 2017;7(12):370–8.

13. de Bruin-Dickason CN, Deacon GB, Forsyth CM, Hanf S, Heilmann OB, Hinton BRW, Junk PC, Somers AE, Tan YQ, Turner DR. Synthesis and structures of rare earth 3-(4′-methyl-benzoyl)-propanoate complexes: new corrosion inhibitors. Aust J Chem. 2017;70(5):478–84.

14. Fan Z, Hou YF, Wang SP, Yang ST, Zhang JJ, Shi SK, Geng LN. Synthesis, crystal structure, and magnetic property of new trispin Ln(III)-nitronyl nitroxide complexes. Helv Chim Acta. 2016;99(9):732–41.

15. Jin CW, Wang Y, Xu SL, Zang JJ. Synthesis, crystal structures and thermochemical properties of ternary rare earth complexes based on 3,4-diethoxybenzoic acid and 2,2′-bipyridine. Acta Phys Chim Sin. 2016;32(9):2232–40.

16. Gao XS, Jiang X, Yao C. Two new complexes of Lanthanide(III) ion with the N_3O_2-donor Schiff base ligand: synthesis, crystal structure, and magnetic properties. J Mol Struct. 2016;1126:275–9.

17. Wang Y, Shen PP, Ren N, Zhang JJ, Geng LN, Wang SP, Shi SK. A series of lanthanide complexes with different N-donor ligands:

18. Hojnik N, Kristl M, Golobič A, Jagličić Z, Drofenik M. The synthesis, structure and physical properties of lanthanide(III) complexes with nicotinic acid. Cent Eur J Chem. 2013;12(2):220–6.

19. Shen PP, Zhu MM, Ren N, Zhang JJ, Wang SP. Four novel lanthanide complexes with 4-ethylbenzoic acid and 5,5′-dimethy-2,2′-bipyridine: structures, luminescent, thermal properties and bacteriostatic activities. Appl Organometal Chem. 2017;31:1–11.

20. Slathia G, Bamzai KK. Growth, structural, optical, thermal and dielectric properties of lanthanum chloride-thiourea-L tartaric acid coordinated complex. Mater Res Express. 2017;4(11):115801–13.

21. Kanchana P, Packiaraj S, Pushpaveni A, Govindarajan S. Isolation, spectroscopic and thermal properties of hydrazinium tris(oxydiacetato)lanthanate(III) hemi(pentahydrate). J Therm Anal Calorim. 2017;129(1):3–14.

22. Luo GH, Gao XH, Pan L, Lv XC, Tan ZC. Low-temperature molar heat capacities and thermodynamic properties of a new rare earth complex $Er_2(\mu 2\text{-Gly})_6(H_2O)_4 \cdot Na_2(ClO_4)_8(H_2O)_2 \cdot 4H_2O$. J Therm Anal Calorim. 2016;126(2):871–9.

23. Pan L, Gao XH, Lv XC, Tan ZC. Low-temperature molar heat capacity and thermodynamic properties of rare earth complex. J Therm Anal Calorim. 2015;124(1):429–35.

24. Zhang JN, Wang H, Tan ZC, Liu BP, Shi Q, Tong B. Low-temperature heat capacities of crystalline $Ho(Gly)_3Cl_3 \cdot 3H_2O$ from 78 to 348 K. J Rare Earth. 2009;27(6):919–22.